Graphical Abstract

A robust and well-balanced finite volume solver for investigating the effects of tides on water renewal timescale in the Nador lagoon, Morocco

Ismail Oubarka, Imad Kissami, Imad Elmahi, Eric Deleersnijder

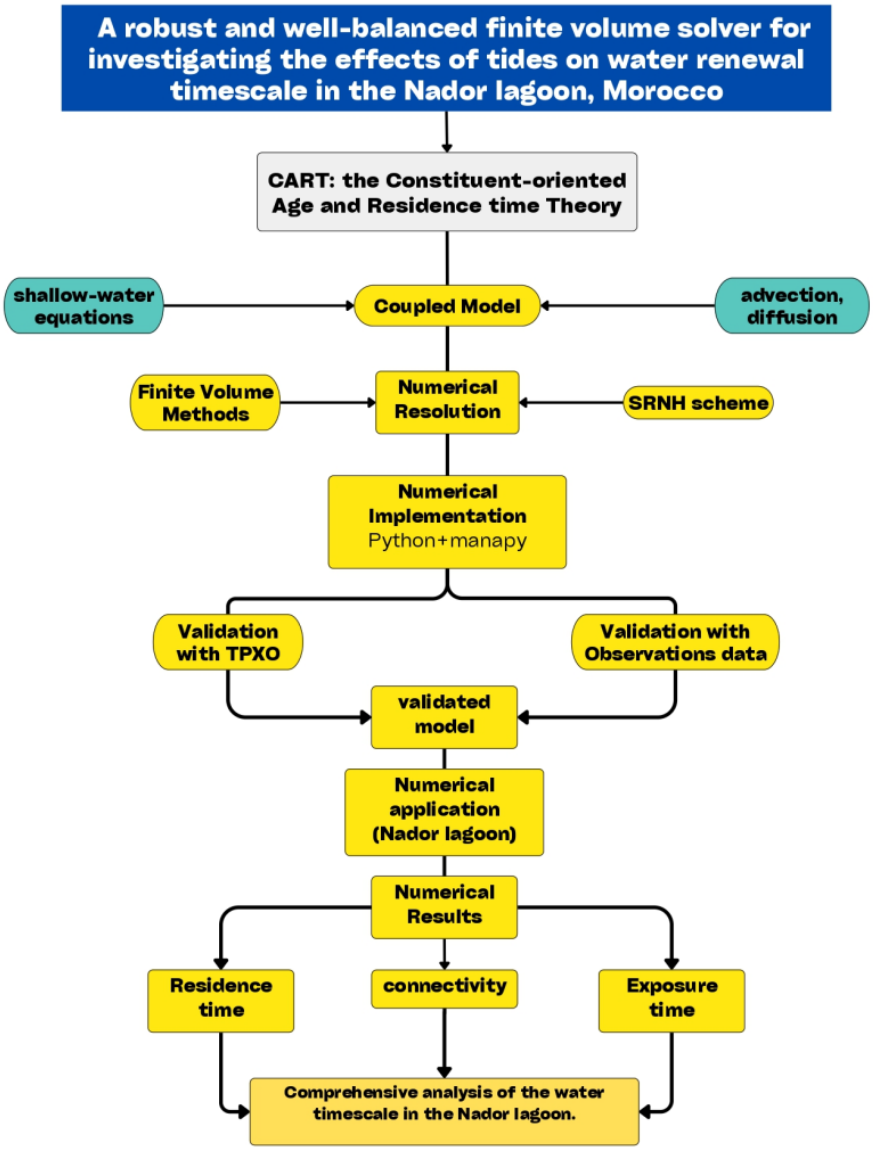

A robust and well-balanced finite volume solver for investigating the effects of tides on water renewal timescale in the Nador lagoon, Morocco

Ismail Oubarka[a,*], Imad Kissami[a], Imad Elmahi[a,b], Eric Deleersnijder[c]

[a] *College of Computing, Mohammed VI Polytechnic University, Lot 660, Ben Guerir, 43150, Morocco*
[b] *ENSAO, LMCS, Mohammed I University, B.P. 669, Oujda, 60000, Morocco*
[c] *Université Catholique de Louvain, IMMC and ELI, B-1348, Louvain-la-Neuve, 1348, Belgium*

Abstract

Coastal lagoons, particularly those not well-connected to the sea, are highly susceptible to continuous water retention, adversely affecting water quality and ecosystems. Understanding and quantifying the processes governing water renewal in such semi-enclosed regions is crucial. Using the principles of constituent-oriented age and residence time theory (www.climate.be/cart), we calculated timescales to explain the water renewal process in semi-enclosed areas. To improve our understanding and define the dynamics of the Nador lagoon, we use two distinct time scales: residence time and exposure time. Residence time indicates the length of time a parcel of water leaves the region of interest for the first time, while exposure time represents the overall length of time a parcel of water remains in that region, including any subsequent inflows. The modeling system adopts an Eulerian approach, including two interlinked model components: the shallow-water equations incorporating bottom friction, eddy viscosity, wind shear stresses, momentum diffusion, and Coriolis forces for modeling hydrodynamics, and a transport-diffusion equation utilized to simulate the advection and diffusion of the passive tracer concentration. The entire system is integrated into a high-order finite volume solver that employs unstructured meshes, upwind numerical fluxes, and slope limiters to achieve precise resolution of steep bathymetric gradients

*Corresponding author
Email address: ismail.oubarka@um6p.ma (Ismail Oubarka)

that may arise in the approximate solution. The scheme is non-oscillatory and preserves the conservation properties. In this research, we explore various situations related to the connection between the Mediterranean Sea and the Nador lagoon. Specifically, we suggest novel entry points that have the potential to significantly decrease the water residence within the lagoon.

Keywords: Finite-volume, Unstructured mesh, PDEs, SRNH, Residence time, Exposure time, Water renewal, Environmental fluid flows, Diagnostic timescales, Tides.

---

1. Introduction

Coastal lagoons, which are critical ecological and economic systems, face significant challenges due to pollutant accumulation, especially when access to adjacent seas is limited. Such accumulation can have long-term negative impacts on water quality and local ecosystems. Understanding the water renewal mechanisms within these lagoons, including determining the residence time the duration water particles remain before exiting to the ocean is crucial for managing these impacts [1, 2, 3, 4].

Environmental studies frequently treat water as a continuous medium, using advection-diffusion equations to monitor water masses by tagging relevant water particles [5, 6, 7]. These studies provide a framework for distinguishing between original water, which was present at the start, and replacement water, which flows into the lagoon from nearby areas.

The shallow water equations (SWE) have contributed significantly to the understanding of these processes. García-Navarro et al. [8] used these equations to model sediment transport over erodible beds in environments with transient flow and movable boundaries. They highlighted their relevance for coastal lagoon water renewal . Thiry et al. [9] combined rotating shallow-water and quasi-geostrophic equations to provide new insights into ageostrophic velocities, which are crucial for predicting water movement in such ecosystems. Fourniotis et al. [10] and Jiang [11] studied how tidal manipulations and wind-driven circulations affect water residence times, leading to a better understanding of lagoon dynamics.

Building on these foundational studies, we present a novel approach using depth integrated equations designed specifically to manage the dynamics of the original water, improving the accuracy of renewal assessments in coastal lagoons. We also introduce two distinct timescales residence and exposure

times to provide a more nuanced understanding of water movement, particularly in tidal systems where water parcels can repeatedly leave and re-enter the lagoon.

Our methodology combines the shallow-water equations with a transport equation to model passive tracers, resulting in a hyperbolic system of conservation laws that are solved using a finite volume approach on unstructured meshes. Incorporating a Non-Homogeneous Riemann Solver (SRNH), that can handle topographical variations, improves advection modelling and enhances our ability to simulate complex coastal environments [12, 13, 14].

As a real application, we focus on the Nador lagoon (see [1]Figure 1) which is located on the North-East of Morocco. The Nador lagoon is an important biological and economic habitat spanning over 120 km^2 with a maximum depth of $8m$, it is influenced by both Mediterranean inflows via the "Bokhana" inlet and a variety of anthropogenic discharges. This study aims to clarify the effect of the inlet's position on the amount of time water remains in the lagoon. It predicts that increased interactions with the Mediterranean Sea will result in a significant decrease in this duration; however, the magnitude of the reduction will vary depending on the specific subdomain being studied. A comprehensive numerical study will determine the need and best positions for more connections between the lagoon and the Mediterranean Sea, thus establishing a strategic foundation for enhancing water quality and ecosystem health [15, 16, 17].

The paper is organized as follows: Section 2 describes the hydrodynamic modelling framework, which uses shallow water equations to better understand the lagoon's fundamental dynamics. Section 3 expands on water renewal timescales, focusing on residence and exposure times, and introduces the Connectivity Matrix for evaluating interactions between subdomains. Section 4 summarizes the finite volume discretization and Non-Homogeneous Riemann Solver, that were used here. Section 5 describes the numerical setup and mesh configurations, followed by an analysis and discussion of simulated results. The paper concludes with a summary of key findings and implications for environmental management and future research directions.

[1]https://planetgallery.global.ssl.fastly.net/full/nador-20170103-full.jpg

Figure 1: This satellite illustration depicts the current condition of the Nador lagoon, highlighting both its state and the position of its inlet.

2. Hydrodynamics Model

The Shallow Water Equations (SWE) are derived from the mathematical model by vertically integrating the incompressible Navier-Stokes equations and incorporating assumptions about hydrostatic pressure and a uniform horizontal velocity profile. Taking into account the impact of wind, Coriolis forces, and bottom friction in the model, the resulting $2D$ equations can be written as follows

$$\begin{cases} \frac{\partial h}{\partial t} + \frac{\partial (hu)}{\partial x} + \frac{\partial (hv)}{\partial y} = 0, \\ \frac{\partial}{\partial t}(hu) + \frac{\partial}{\partial x}(hu^2 + \frac{gh^2}{2}) + \frac{\partial}{\partial y}(huv) = -gh\frac{\partial Z}{\partial x} + \frac{\tau_{wx} - \tau_{bx}}{\rho_w} + f_c hv + \mathcal{D}_{xx}(h,u,v) \\ \frac{\partial}{\partial t}(hv) + \frac{\partial}{\partial x}(huv) + \frac{\partial}{\partial y}(hv^2 + \frac{gh^2}{2}) = -gh\frac{\partial Z}{\partial y} + \frac{\tau_{wy} - \tau_{by}}{\rho_w} - f_c hu + \mathcal{D}_{yy}(h,u,v) \end{cases} \tag{1}$$

The unknowns of the equations are the positive water height $h(t,x,y) > 0$ and the mean horizontal velocity $u(t,x,y) := (u,v)^T(t,x,y) \in \mathbb{R}^2$, with Z representing the bottom topography. The parameter f_c is intricately connected to the Earth's angular speed and is defined as $f_c = 2\omega \sin(\phi)$, where ω stands for the angular velocity of the earth, ϕ denotes the geographic latitude, and ρ_w signifies the density of water. The bed shear stresses τ_{bx} and τ_{by} in the x and y directions are expressed as

$$\tau_{bx} = \rho_w C_b u\sqrt{u^2+v^2}, \qquad \tau_{by} = \rho_w C_b v\sqrt{u^2+v^2} \tag{2}$$

The topography friction coefficient, denoted as C_b, can either be a constant or determined by $C_b = g/C_z^2$, where $C_z = h^{\frac{1}{6}}/n_b$ is the Chezy constant, and n_b represents the Manning coefficient at the bottom. The surface stress τ_w generally arises from wind shear and is formulated as a quadratic function of wind speed.

$$\tau_{wx} = \rho_w C_w w_x \sqrt{w_x^2 + w_y^2}, \qquad \tau_{wy} = \rho_w C_w w_y \sqrt{w_x^2 + w_y^2} \tag{3}$$

where $w = (w_x, w_y)^T$ represents the speed of the wind at $10m$ above the water surface, and C_w is the wind friction coefficient given by Garratt formula [18] (see also [19] for a review of wind stress calculation techniques):

$$C_w = \rho_a \left(0.75 + 0.067\sqrt{w_x^2 + w_y^2}\right) 10^{-3} \tag{4}$$

where ρ_a denotes air density.

The viscous terms in the shallow water equations are generally derived by averaging the incompressible Navier-Stokes equations based on standard shallow water assumptions. The selection of these viscous terms is in fact a critical aspect of accurate modeling of shallow water flows and a clear and clean derivation of these viscous terms can be found in the first chapter of the book by Zhou [20]. However, this standard averaging of shallow water equations does not take into account first order terms. Thus, in the model considered in our study, we used the derivation developed by Gerbeau and Perthame [21] for 1D and extended by Marche [22] for 2D, who used a second order expansion to obtain an averaged shallow water equations with viscosity. The momentum diffusion terms $D_{xx}(h, u, v)$ and $D_{yy}(h, u, v)$ are expressed as

$$\begin{aligned} \mathcal{D}_{xx}(h, u, v) &= 2\nu \frac{\partial}{\partial x}\left(h\left(2\frac{\partial u}{\partial x} + \frac{\partial v}{\partial y}\right)\right) + 2\nu \frac{\partial}{\partial y}\left(h\frac{\partial u}{\partial y}\right) \\ \mathcal{D}_{yy}(h, u, v) &= 2\nu \frac{\partial}{\partial x}\left(h\frac{\partial v}{\partial x}\right) + 2\nu \frac{\partial}{\partial y}\left(h\left(\frac{\partial u}{\partial x} + 2\frac{\partial v}{\partial y}\right)\right) \end{aligned} \tag{5}$$

Here, ν stands for kinematic viscosity.

Note that in this study, we have assumed the flow is in the laminar regime. However, the model (1) can be adapted to include turbulent effects by adjusting the eddy viscosity. Additionally, (3) permits the use of different coefficients of wind friction, as explored in various studies [23, 24].

3. Water Renewal Timescales

3.1. Residence time

Let $\Omega \subset \mathbb{R}^2$ denote the region of interest, which represents here the Nador lagoon. The residence time in a subdomain Ω' of Ω at time $t = t_0$ refers to the time it takes by a water parcel, initially within $\Omega^{'}$, to exit that region for the first time. To determine the residence time, the following partial differential equation needs to be solved by coupling it with equations (1), regarding the initial and boundary conditions [25]

$$\begin{cases} \frac{\partial}{\partial t}(hC) \,+\, \nabla \cdot (hC\mathbf{u}) \,=\, \nabla \cdot (h\mathbf{K}\nabla C) \\ \\ C(t_0, \mathbf{x} \in \Omega^{'}) \,=\, 1 \\ C(t_0, \mathbf{x} \in \Omega \setminus \Omega^{'}) \,=\, 0 \end{cases}, \tag{6}$$

where h refers to the water height, $\mathbf{x}$ the horizontal coordinates (x, y), $\mathbf{u}$ the velocity vector, and $\mathbf{K}$ the diffusivity tensor. The criterion for water entering the specified area after t_0 requires it to have no tracer. Furthermore, the tracers that escape through the open boundaries are permanently lost and cannot re-enter the region of interest $C(t, \mathbf{x} \in \Gamma^{inlet}) = 0$. The absence of water particle movement across the coastline boundary, denoted Γ^c, results in the following no-flux boundary condition

$$\left[(hC\mathbf{u} - h\mathbf{K}\nabla C) \cdot \mathbf{n}\right]_{\mathbf{x} \in \Gamma^c} \,=\, 0.$$

Assuming the utilization of a two-dimensional depth-averaged model, the residence time of water at t_0 present in $\Omega^{'}$ equivalent to

$$\overline{\theta}(t_0) \,=\, \frac{\int_{t_0}^{\infty} \int_{\Omega} h(t, \mathbf{x})\, C(t, \mathbf{x})\, d\mathbf{x}\, dt}{\int_{\Omega} h(t_0, \mathbf{x})\, C(t_0, \mathbf{x})\, d\mathbf{x}} \,=\, \frac{\int_{t_0}^{\infty} \int_{\Omega} h(t, \mathbf{x})\, C(t, \mathbf{x})\, d\mathbf{x}\, dt}{\int_{\Omega'} h(t_0, \mathbf{x})\, d\mathbf{x}}, \tag{7}$$

In practical terms, calculating the residence time for water within region $\Omega^{'}$ at t_0 involves simulating $C(t, x)$ (as shown in Equation (6)) and $h(t, x)$ over an extended period until the majority of the tracer has exited the region of interest Ω. This extended simulation ensures that the residence time estimate has reached convergence. Once this convergence is achieved, the integrals in Equation (7) can be evaluated to determine the mean residence time accurately.

3.2. Exposure time

Using residence time as a gauge for water replenishment has conceptual limitations since it neglects instances of water returning to the area of interest. This constraint is particularly noticeable in tidal systems, where segments of water frequently leave and re-enter the domain before eventually escaping, which leads to unrealistic timescales. To tackle this issue, the concept of exposure time, as introduced by [26, 3], offers a more accurate timescale in such scenarios. Exposure time and residence time share similarities, encompassing the definition of the region of interest, and the initial time. However, the numerical computation of exposure times necessitates a larger simulation domain that includes the areas where water enters the domain of interest. This ensures that the returned water parcels are explicitly considered.

In any given scenario, computing residence time and exposure time for a specific configuration allows for a comparison between these two measures. Analyzing the difference between exposure time and residence time provides valuable insights into the contribution of re-entering water to the exposure time. If the residence time is equal to the exposure time, this indicates that no water particles that leave the area of interest return to it. The return coefficient, representing the relative difference between exposure time (ET) and residence time (RT), is calculated using the following equation

$$r_c = \frac{ET - RT}{ET}. \tag{8}$$

With this description, the return coefficient r_c is in the range 0 to 1. If there is no backflow, the exposure time ET is equal to the residence time RT, giving $r_c = 0$. At the other extreme, $r_c = 1$ occurs when the residence time is significantly smaller than the exposure time, indicating that the water leaves the zone of interest quickly but spends a long time thereafter re-entering several times.

3.3. Connectivity Matrix

Residence and exposure times are calculated for various initial regions, typically achieved by dividing the area of interest into multiple subdomains. In such cases, an additional time diagnosis becomes precious since it measures the duration of a parcel of water, present initially in sub-domain i, remains in each sub-domain $j \in \{1, ..., n\}$.

This measure allows for the identification of significant connections between subdomains, offering a general understanding of where the water discharged from various locations tends to linger during its journey outside the area of interest. This eliminates the need to delve into intricate circulation and transport patterns. Similar to the meaning of residence time for the entire area of interest in equations (9), the notion of subdomain exposure time $\Theta_{ij}(t_0)$ is expressed as follows

$$\Theta_{ij}(t_0) \;=\; \frac{\int_{t_0}^{\infty}\int_{\Omega_j} h(t,\mathbf{x})\, C_i(t,\mathbf{x})\, d\mathbf{x}\, dt}{\int_{\Omega_i} h(t_0,\mathbf{x})\, d\mathbf{x}} \tag{9}$$

for the duration spent in subdomain j by water initially in subdomain i. This implies that $\Theta_{ij}(t_0)$ indeed denotes a subdomain exposure time containing all stays in the sub-domain. In the specific case $i = j$, $\Theta_{ij}(t_0)$ is the exposure time of box i, depicting the overall time spent in the initial box i.

The quantity without dimension represents the ratio between the time spent by the particles in the sub-domain Ω_j and the total time they spend in the region of study Ω, given that they were initially present in the sub-domain Ω_i expressed using the following formula

$$d_{ij} = \frac{\Theta_{ij}(t_0)}{\Theta_i(t_0)} = \frac{\Theta_{ij}(t_0)}{\sum_{j=1}^{n}\Theta_{ij}(t_0)} \tag{10}$$

It is obvious that $\sum_{j=1}^{n} d_{ij} = 1$, which indicates that when the value of d_{ij} is close to 1, particles in the subdomain Ω_i spend a large amount of time in the subdomain Ω_j. In simpler terms, most of the overall time these particles stay within the region of interest is allocated to Ω_j. These d_{ij} values collectively form a matrix recognized as the connectivity matrix. This matrix serves as a visualization of the connections between various subregions within the domain of interest.

4. Finite volume discretization and Non-Homogeneous Riemann Solver

In this section, we provide a brief overview of the numerical method used to solve equations (1) and (6) and we direct readers to references [6, 7, 12] for more detailed information.

4.1. Formulation of the method

Equations (1)-(6) can be expressed in the following conservative form

$$\frac{\partial \mathbf{W}}{\partial t} + \frac{\partial}{\partial x}\left(\mathbf{F}(\mathbf{W}) - \widetilde{\mathbf{F}}(\mathbf{W})\right) + \frac{\partial}{\partial y}\left(\mathbf{G}(\mathbf{W}) - \widetilde{\mathbf{G}}(\mathbf{W})\right) = \mathbf{S}_1(\mathbf{W}) + \mathbf{S}_2(\mathbf{W}), \tag{11}$$

$\mathbf{W}$ is the vector of conserved variables, ($\mathbf{F}$,$\mathbf{G}$) and ($\widetilde{\mathbf{F}}$,$\widetilde{\mathbf{G}}$) are the advective and diffusion tensor fluxes, and $\mathbf{S_1}$ and $\mathbf{S_2}$ are the source terms due to slope variations, bottom friction losses, Coriolis forces and wind effects.

Discretizing the computational domain in control volumes, the finite volume method applied to system (11) results in

$$\mathbf{W}_i^{n+1} = \mathbf{W}_i^n - \frac{\Delta t}{|T_i|}\sum_{j\in N(i)}\int_{\Gamma_{ij}} \mathcal{F}\left(\mathbf{W}^n;\mathbf{n}\right)\mathrm{d}\sigma + \frac{\Delta t}{|T_i|}\sum_{j\in N(i)}\int_{\Gamma_{ij}} \widetilde{\mathcal{F}}\left(\mathbf{W}^n;\mathbf{n}\right)\mathrm{d}\sigma \tag{12}$$

$$+\frac{\Delta t}{|T_i|}\int_{T_i}\left(\mathbf{S}_1(\mathbf{W}^n) + \mathbf{S}_2(\mathbf{W}^n)\right)\mathrm{d}V$$

where $\mathbf{W}_i^n$ is the mean value of the solution $\mathbf{W}$ in the control volume T_i at time t_n, $|T_i|$ represents the area of T_i, Γ_{ij} is the edge of the mesh triangle, and $N(i)$ is the set of triangles surrounding the cell T_i,

$$\mathcal{F}(\mathbf{W};\mathbf{n}) = \mathbf{F}(\mathbf{W})n_x + \mathbf{G}(\mathbf{W})n_y \qquad \widetilde{\mathcal{F}}(\mathbf{W};\mathbf{n}) = \widetilde{\mathbf{F}}(\mathbf{W})n_x + \widetilde{\mathbf{F}}(\mathbf{W})n_y$$

$$\mathbf{W}_i^n = \frac{1}{|T_i|}\int_{T_i}\mathbf{W}^n\,\mathrm{d}V.$$

The SRNH scheme consists of predictor and corrector steps. In the predictor step, the state variable $\mathbf{W}_{ij}^n$ on every edge Γ_{ij} is determined through an upwind scheme that solves a Riemann problem, expressed as flows

$$\mathbf{W}_{ij}^n = \frac{1}{2}\left(\mathbf{W}_i^n + \mathbf{W}_j^n\right) - \frac{1}{2}\mathbf{sgn}\left[\nabla\mathcal{F}(\overline{\mathbf{W}}_{ij}^n,\mathbf{n}_{ij})\right]\left(\mathbf{W}_j^n - \mathbf{W}_i^n\right) + \frac{1}{2}|\nabla\mathcal{F}(\overline{\mathbf{W}}_{ij}^n,\mathbf{n}_{ij})^{-1}|\mathbf{S}_{1ij}^n, \tag{13}$$

$$\mathbf{S}_{1i}^n = \frac{1}{|T_i|}\int_{T_i}\mathbf{S}_1(\mathbf{W}^n)\,dV, \tag{14}$$

where $\mathbf{sgn}$ represents the sign matrix and $\overline{\mathbf{W}}_{ij}^n$ is the averaged state that can be roughly approximated by the mean state or the Roe's average state.

$$\overline{\mathbf{W}}_{ij}^n = \frac{1}{2}\left(\mathbf{W}_i^n + \mathbf{W}_j^n\right).$$

In the corrector step, the state variables at time t^{n+1} are updated based on the physical flux on the predicted states as follows

$$\mathbf{W}_i^{n+1} = \mathbf{W}_i^n - \frac{\Delta t}{|T_i|} \sum_{j \in N(i)} \mathcal{F}\left(\mathbf{W}_{ij}^n; \mathbf{n}_{ij}\right) |\Gamma_{ij}| + \Delta t \mathbf{S}_{1i}^n, \tag{15}$$

The detailed formulation of the approximation of the sign matrix and the source term in (13) and (15) are provided in [12], and will not be repeated here. The discretization of this source term was designed to satisfy the well-known C-property. The discretization of the diffusion fluxes in Eq. (12) is performed using a Green-Gauss diamond reconstruction. For further details, please refer to [7].

4.2. Boundary conditions

4.2.1. Treatment of the flux at the boundaries

The SRNH scheme applies similar techniques to handle boundary conditions as described in reference [7]. In the computational examples considered in this paper, boundary conditions are imposed on the corrector solution by computing fluxes at the boundaries. For the predictor solution and the slopes of dependent variables, boundary conditions are enforced within boundary cells by setting the required variables to the corresponding values of the adjacent inner cells. When slopes are calculated based on vertex values, the solution at boundary vertices is determined by interpolation from two neighboring centroids. In contrast, when slopes are computed based on centroid values, the three points used to estimate the slopes consist of the centroid and the two neighboring centroids within the computational domain. For more details on the implementation of boundary conditions for the SRNH scheme, please refer to references [27].

4.2.2. Open boundary conditions

The Flather condition, initially introduced by Flather in 1976 [28], extends a radiation boundary condition that belongs to a well-known category of open boundary conditions (OBCs). It is based on the propagation of a quantity represented as ψ through a boundary

$$\frac{\partial \psi}{\partial t} + c \frac{\partial \psi}{\partial n} = 0 \tag{16}$$

where n represents the outward normal. The Flather condition combines (16), which is applied to the free surface elevation, with the long wave phase

speed ($c = \sqrt{gh}$). Additionally, it involves a one-dimensional approximation of the continuity equation

$$\frac{\partial \eta}{\partial t} + h\frac{\partial \bar{v}_n}{\partial n} = 0 \quad which \quad gives \quad \frac{\partial}{\partial n}\left[\bar{v}_n - \frac{c}{h}\eta\right] = 0.$$

In conclusion, performing the integration across the boundary results in

$$\bar{v}_{n,b} = \bar{v}_n^{\text{ext}} \pm \sqrt{\frac{g}{h}}\left(\eta_{b\pm1} - \eta^{\text{ext}}\right).$$

5. Numerical results

5.1. Numerical setup

The Nador lagoon is located along Morocco's Mediterranean coastline, approximately at $35°N$ coordinate (refer to Figure 2). With a total surface area of $115\,km^2$ and a volume of approximately $542\,Mm^3$, the lagoon plays a crucial role in our analysis. The mesh of the computational domain is illustrated in Figure 2, containing a total of 73322 elements and 36612 nodes. Notably, node density is higher at the lagoon level to ensure precision within this specific region of interest. This strategic emphasis on accuracy is also associated with our detailed coastline refinement. The objective is to attain a suitable density of points between the coastal borders and the sea, facilitating accurate treatment of boundary conditions. Our study requires the implementation of two distinct boundary conditions at the open boundaries, both western and eastern. These conditions encompass tidal forces and flow currents, derived from the TPXO model [29]. An essential aspect is the model spin-up, which involves a year-long hydrodynamic modeling process to establish flow patterns. The initial conditions for our study are based on the resulting water height and velocity fields. Subsequently, the Nador lagoon is subjected to a complete release of tracer with an initial concentration set at 1.

Within this research, we investigate four distinct scenarios. The first scenario involves establishing a new inlet (Boukhana) to connect the Nador lagoon with the sea. The second scenario focuses exclusively on the old inlet of the lagoon; the third scenario considers the old and new inlets simultaneously; and the last scenario incorporates two new smaller inlets near "Beni-Ansar" and "Kariat-Arekmane". Figure (2) provides a visual representation of these three inlet configurations. Additionally, the depiction of the

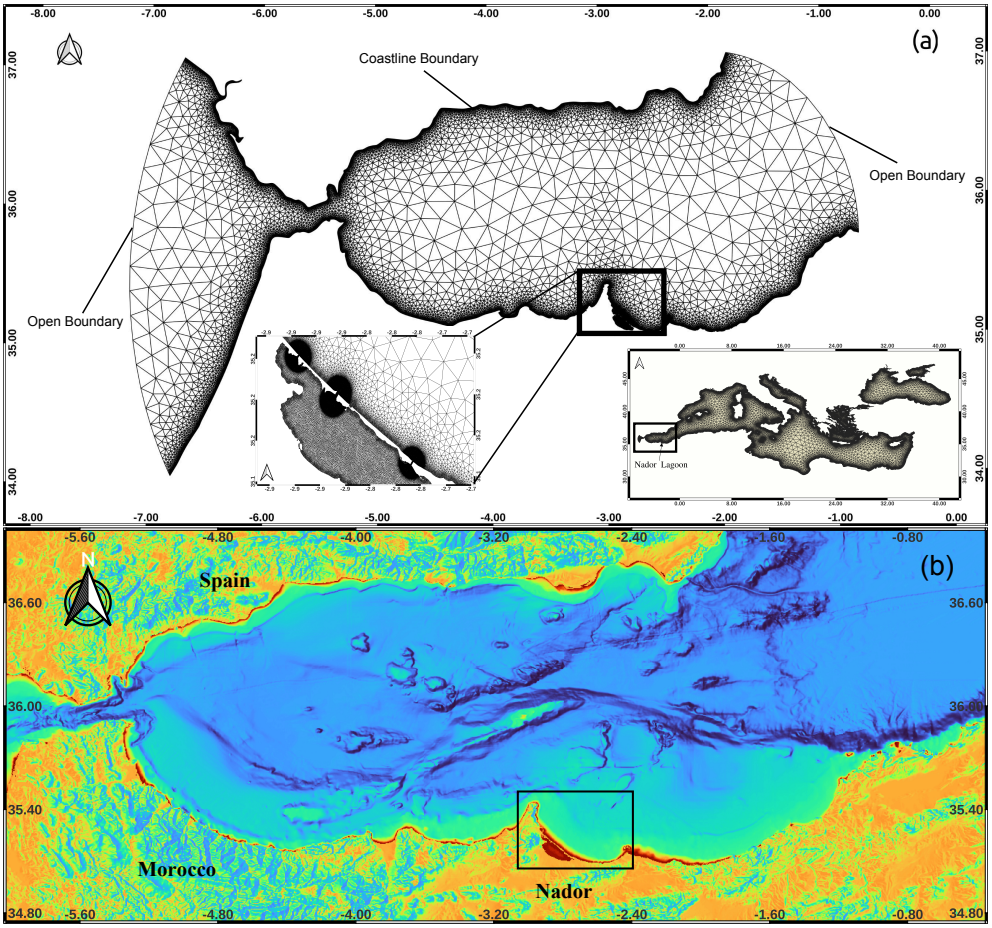

Figure 2: Computational domain grid depicting latitude and longitude in degrees: (a) displays the entire computational mesh, while zooming on the Nador lagoon highlights the connection between the lagoon and the sea; (b) provides a bathymetric overview, illustrating the topography of the study area.

underwater topography of the Nador lagoon, as shown in Figure (2) (b), was obtained from various datasets compiled from 2001 to 2018. We gathered this information through both single and multi-beam echo soundings. The bathymetric details for the surrounding sea area were obtained from the EMODnet portal (http://portal.emodnet-bathymetry.eu), originating from the GEBCO dataset. The parameters and reference quantities selected for evaluating the current model are summarized in Table 1. The full numerical model was implemented using Manapy [30] (https://github.com/imadki/manapy),

a parallel Python-based tool that utilizes an object-oriented, unstructured finite-volume solver for the resolution of partial differential equations.

Table 1: Parameters and reference quantities considered in the present study.

Quantity	Reference value
ρ_w	$10^3 \mathrm{kg/m}^3$
ρ_a	$1.293 \mathrm{kg/m}^3$
g	$9.81 \mathrm{m/s}^2$
ν	$10^{-6} \mathrm{m}^2/\mathrm{s}$
$\mathbf{K}$	$2 \times 10^{-9} \mathrm{m}^2/\mathrm{s}$
n_b	$2.5 \times 10^{-3} \mathrm{s/m}^{1/3}$
ω	$7.272 \times 10^{-5} rad/s$

5.2. Convergence test

Because of the non-linearity of the system of partial differential equations to be solved, the analytical solution cannot be found explicitly. Instead of using the analytical solution, we create a reference numerical solution by computing on very fine mesh consisting of about 5 million elements. This reference solution is then used to perform the convergence test of the numerical scheme on three different meshes. The obtained results for the relative L^2 error in the water height and the passive tracer concentration are listed in Table 2 along with the corresponding CPU times to achieve a physical time of 10 days.

Table 2: The relative error in the L^2-norm for the variables h and C. The CPU time for 1 core is given in days, while the CPU time for 112 cores is given in hours.

# of elements	Variable	$t = 1$ day	$t = 5$ days	$t = 10$ days	Timing (days)	Timing (hours)
					1 core	112 cores
248773	h	4.247×10^{-3}	5.348×10^{-3}	5.903×10^{-3}	5.671	1.271
	C	1.185×10^{-2}	3.216×10^{-2}	4.006×10^{-2}		
73322	h	9.167×10^{-3}	2.601×10^{-2}	2.894×10^{-2}	1.864	$0,425$
	C	2.755×10^{-2}	5.425×10^{-2}	6.510×10^{-2}		
21347	h	3.153×10^{-2}	4.934×10^{-2}	7.423×10^{-2}	0.539	0.115
	C	1.630×10^{-1}	7.920×10^{-1}	8.101×10^{-1}		

5.3. Comparison of modeled results with measurements and TPXO's prediction

Measuring timescales such as residence and exposure time presents challenges, often requiring a passive tracer release experiment. This experiment would involve continuous monitoring at various points across the relevant area for weeks or even months. Consequently, validating timescales estimated through computer simulations is highly complicated, as pointed out by Deleersnijder and Delhez [31]. However, this doesn't imply that the model's outcomes are entirely unreliable. The common approach involves validating the hydrodynamics that control the passive tracer transport by comparing them with observed data such as tide elevation and current patterns. This practice assumes that by validating the hydrodynamics, the computed timescales are also indirectly validated, as both are governed by the same transport mechanisms [31]. In this study, the hydrodynamics fields produced by simulations were verified against available observations (TPXO) as well as measured tides at Melilla port for the year 2017. A brief summary of these validation results is presented in Figure 3. These results serve as a primary confirmation of the accuracy of the timescales depicted below. In this section, we provide a comparison of tidal elevations and conduct statistical evaluations of differences between the model's simulations and actual observations. Figures 4 and 3 offer instances of a qualitative comparison across all monitoring stations. Overall, the figures illustrate a strong correspondence between the simulated and observed tidal elevations, as well as a similar pattern for tidal currents. This agreement is reinforced by the accurate prediction of low and high water levels during both neap and spring tidal cycles (as depicted in Figures 3 and 4), along with the accurate replication of various tidal patterns within the sea region.

5.4. Residence time, Exposure time, and Connectivity

The initial goal involved calculating the residence and exposure time within Nador lagoon, followed by a comparison of these outcomes with those documented in [32]. The outcomes of this study's residence and exposure times are depicted in Figure 5 and Table 3. In our instance, the simulations were executed over a minimum period of 3 months, a duration chosen to guarantee that a substantial majority of tracers have left the lagoon. In practical terms, the simulation's conclusion witnessed less than 0.1 of the initial tracer content remaining within the defined area. Analyzing the results depicted

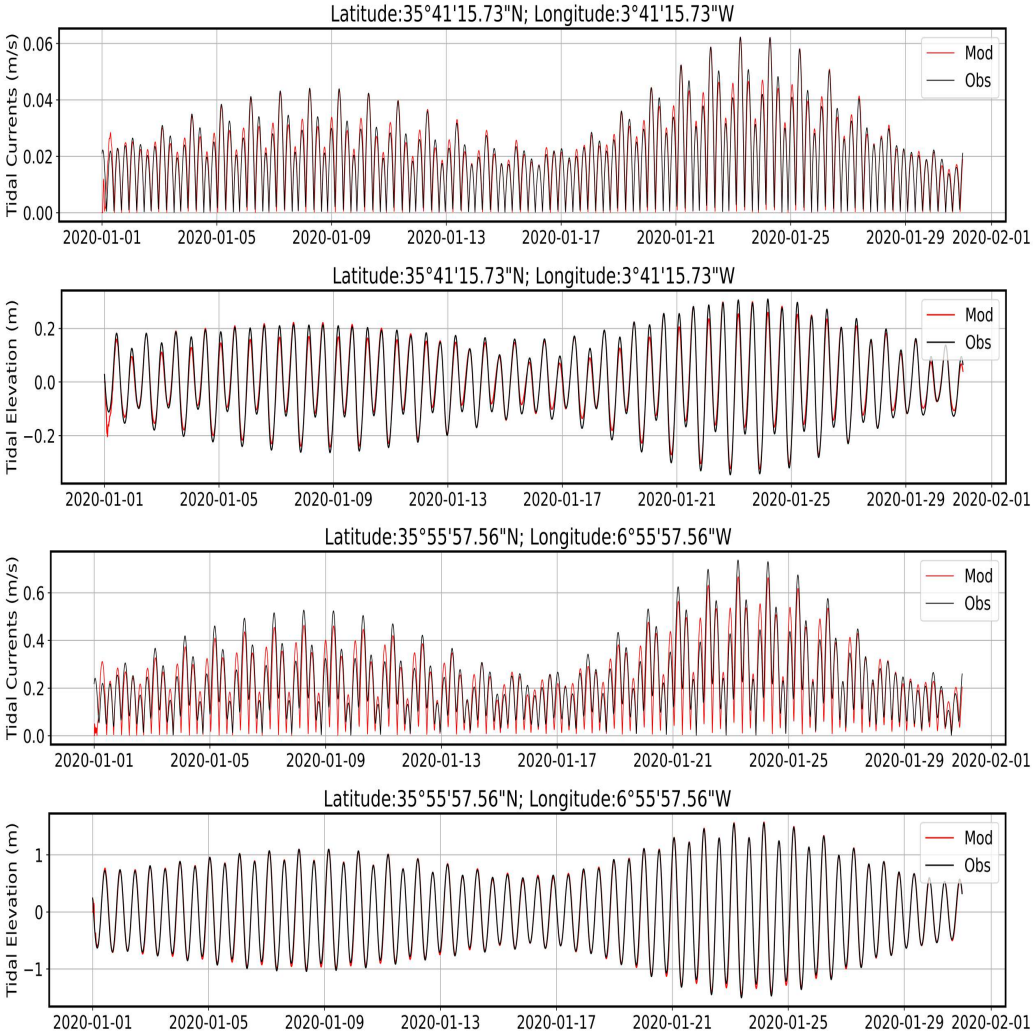

Figure 3: Comparisons between tidal simulation and observations taken from TPXO global model.

in Figure 5 and Table 3, it is clear that both the residence time and exposure time are substantial, particularly with the old pass. Through this old pass, the Nador lagoon undergoes a complete water renewal cycle that lasts nearly 59 days. In contrast, the introduction of the new inlet significantly shortens this duration to just 15 days, aligning with the observations in [32]. Despite the decrease in residence and exposure times caused by the transition from the old inlet to the new one, it is insufficient to ensure immediate

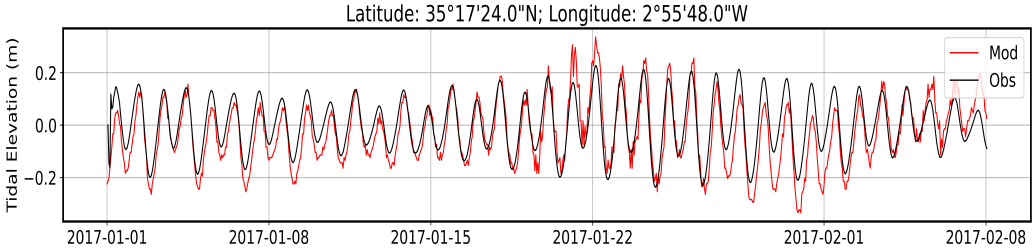

Figure 4: Modeled tides compared to time series measured at the Port of Melilla in January 2017.

Table 3: The mean residence time of the water in the Nador lagoon and the CPU time required for each simulation using a single and multiple cores.

Inlet type	Initial tide	January March	April June	July September	October December	Timing (days) 1 core	Timing (hours) 56 cores
New inlet	high tides	15.58	14.67	16.82	17.36	23.273	8, 280
	low tides	14.16	13.89	15.02	17.14		
Old inlet	high tides	58.43	58.10	57.21	61.37	19.298	5.640
	low tides	57.22	56.73	56.61	59.06		
Two inlets	high tides	23.04	20.25	18, 01	23, 43	18.840	3.486
	low tides	22, 85	20.03	19, 79	22, 74		
Three inlets	high tides	5.34	3.21	4.58	6.58	25.324	13.831
	low tides	3.02	3.36	2.87	6.23		

self-cleaning of the lagoon. In an effort to explore additional possibilities, we experimented with the simultaneous opening of both the new and old inlets. Unfortunately, the results indicate that this approach does not significantly improve the time required for self-cleaning. The timescales remain nearly unchanged. Consequently, rather than depending on the existing inlets in the lagoon, we decided to propose new, smaller inlets near "Bnensar" and "Karyat-Arcman". Examining the outcomes illustrated in Figure 5 and Table 3, it becomes evident that the inclusion of a small inlet alongside the new and old inlets results in a significant reduction in water renewal time of approximately 4 days. This result is a promising indicator, suggesting a more assured achievement of fast self-cleaning for the lagoon. We have divided the Nador lagoon into seven sub-blocks, numbered 1 to 7, from north to south, to understand the influence of tidal forcing on residence times (see Figure 6).

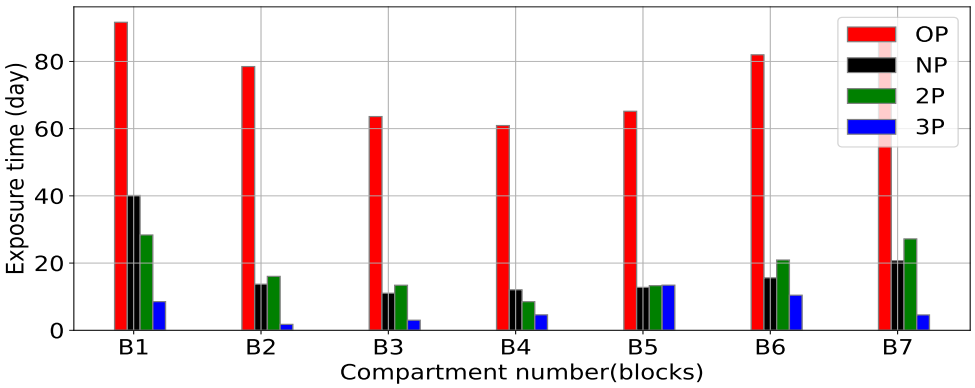

Figure 5: Exposure time outcomes in each block for various scenarios: (NP) New inlet, (OP) Old inlet, (2P) Old and new inlets simultaneously, and (3P) New inlet with the additional proposed small inlets.

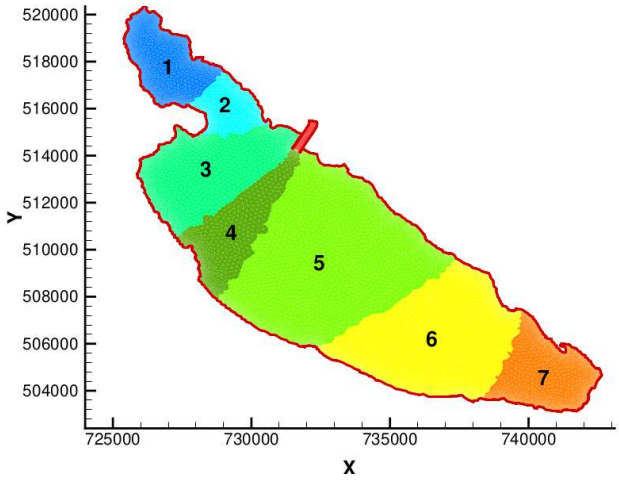

Figure 6: The numbers and distinct colors represent the various blocks in the Nador lagoon.

Segmenting the lagoon into these blocks clears light on the water renewal dynamics within each block. Under the old inlet scenario, all blocks encounter extended renewal times due to the limited impact of small tidal currents reaching them. Moreover, each block's renewal time closely correlates with its distance from the inlet, indicating an increase in both residence and exposure times as the inlet moves farther away. Similar trends emerge in the new inlet scenario, as well as the simultaneous use of new and old inlets. In the

three-inlet scenario, residence and exposure times in all blocks become nearly uniform and notably shorter. This consistent pattern strongly suggests that employing three inlets simultaneously is an effective strategy for reducing timescales in the Nador lagoon. In Figure 8, the distribution of the tracer over time in each block shows how the residence and the exposed times are developed in each block and are depicted for each scenario. The results of the residence and exposure times in the Nador lagoon align with this visualization. Figure 7 depicts the concentration of the tracer distribution after an elapsed period of 11 days. This illustration provides insight into the tracer distribution corresponding to the previously discussed residence and exposed time outcomes. The final results concern the connectivity matrix. This study presents these matrices visually for the four scenarios it examines. Firstly, it is obvious that there is a distinction between the different matrices.

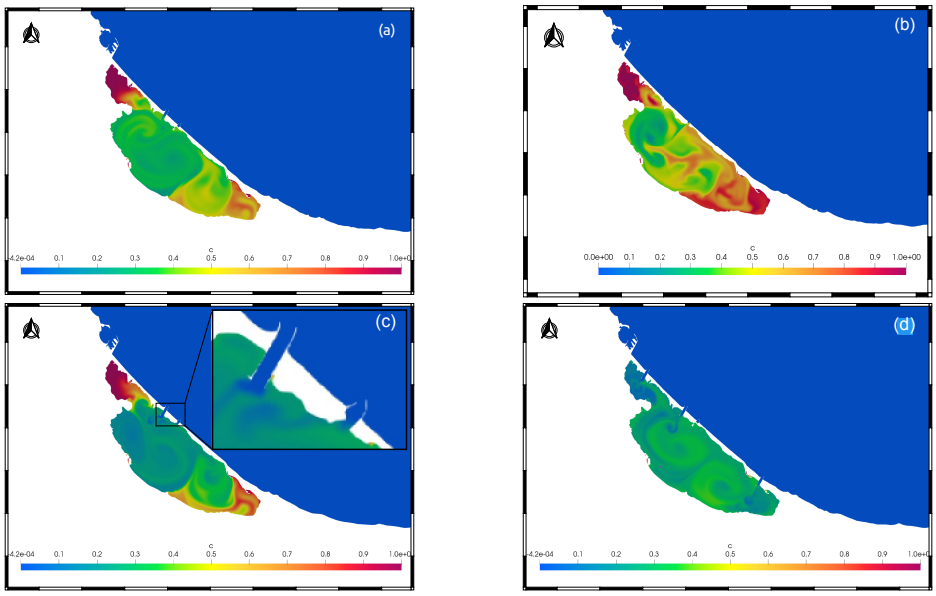

Figure 7: Tracer concentration in Nador lagoon at physical times 11 (day): (a) New inlet, (b) Old inlet,(c) Old and new inlet simultaneously, and (d) New inlet with the additional proposed small inlets.

Therefore, we will focus on general and shared patterns. The connectivity matrix clearly outlines the proportion of exposure time to the Nador lagoon for each sub-block. Therefore, we can observe that water tends to spend relatively more time in some blocks than in others as it progresses out of the lagoon. Water predominantly occupies its original block, as naturally

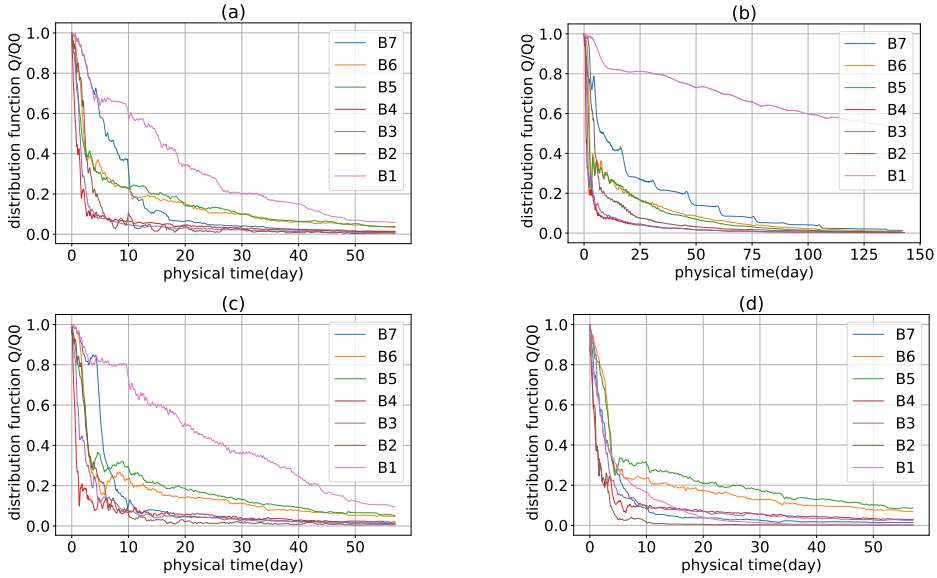

Figure 8: The temporal distribution of the passive tracer, as defined in Eqs (7), within each block 1 through 7 in the Nador lagoon with varied connections to the Mediterranean Sea is illustrated in the following scenarios: (a) New inlet, (b) Old inlet, (c) Old and new simultaneously, and (d) New inlet with the additional proposed small inlets.

expected, especially in blocks 1, 5, 6, and 7. However, in the case of the three inlets, blocks 5 and 6 are interconnected with all the other blocks. This suggests that the water from the entire Nador lagoon passes through these blocks before it exits the lagoon. This discussion highlights how the connectivity matrix serves as a tool for interpreting spatial exposure time variations.

6. Conclusion

In this study, a shallow water flow model coupled to an advection-diffusion equation for a passive tracer, have been used to compute the residence and exposure times in the Nador lagoon. The model was solved using a finite volume method on unstructured triangular meshes. The convective fluxes were approximated by a Non-Homogeneous-Riemann Solver that can handle irregular topography, whereas the diffusion fluxes were performed using a Green-Gauss diamond reconstruction.

While the approach has proven to be useful for investigating water flow and time scales, the use of a passive tracer limits the capacity to cap-

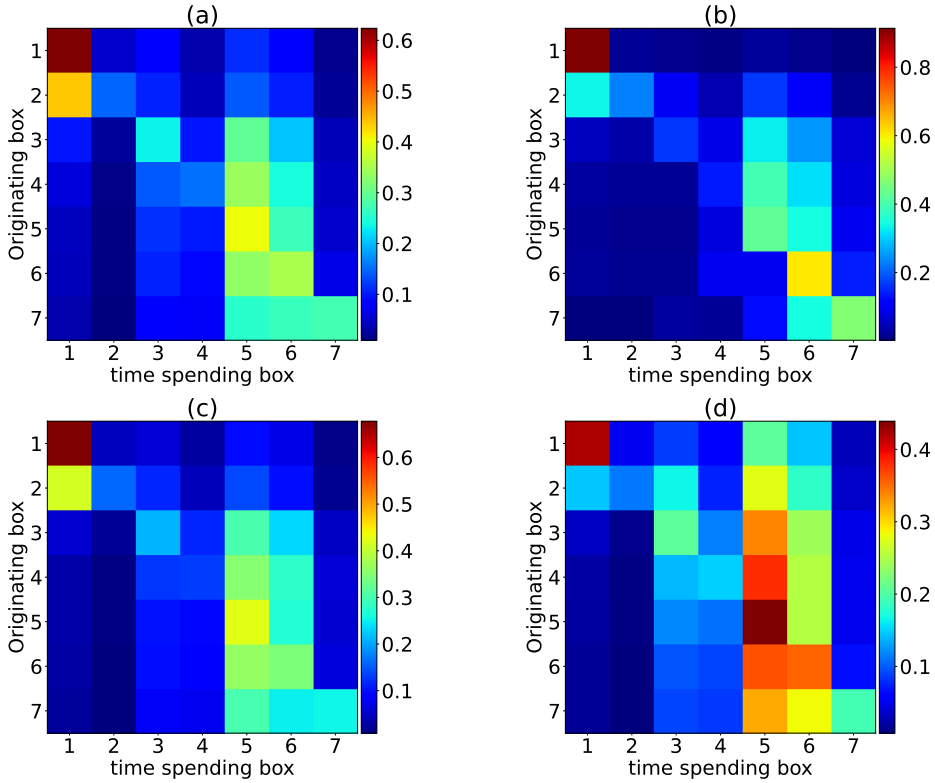

Figure 9: Connectivity matrices, as defined in Equation (10), depict the proportionate time allocation in boxes 1 through 7 by water initially present in boxes 1 through 7. (a) New inlet, (b) Old inlet, (c) Old and new simultaneously, and (d) New inlet with the additional proposed small inlets.

ture the intricate interactions observed in models such as the Nutrient-Phytoplankton-Zooplankton (NPZ). This model tackles the dynamic connections between nutrients, phytoplankton, and zooplankton, which are critical for understanding the ecological effects of certain contaminants such as mercury, lead, chromium, arsenic, and cadmium. Future studies will then aim to incorporate components of the NPZ model or similar frameworks to more precisely replicate the biological and chemical behaviors of these contaminants in aquatic environments.

Moreover, the model used in this study adopts a domain-wide averaging to compute exposure times, which provides a broad picture but does not account for localized changes in water residence times across different regions of the Nador lagoon. To provide more extensive and comprehensive research,

we plan to build a novel method for determining exposure periods that incorporates a two-step process: first, we solve hydrodynamics forward in time to collect data on water height and velocity. This information is then used in a backward step to answer the exposure time equation. Although exact, this strategy necessitates keeping a vast amount of data, which presents considerable computational resource issues. To address these issues, the use of machine learning techniques is being investigated. These techniques will reduce the data storage requirements for the backward step, and thus improve the efficiency and scalability of the model.

Finally, this work represents a significant advance in the understanding and management of environmental processes in the Nador lagoon. By providing a comprehensive perspective and practical insights, it lays the groundwork for future efforts to preserve this essential coastal ecosystem, paving the way for more detailed and comprehensive environmental modeling projects that incorporate real-world pollutants and advanced computational methods.

Acknowledgments

The authors express gratitude to the Toubkal Supercomputer of UM6P [2] for their support in executing numerical computations on their clusters.

References

[1] L. V. Lucas, E. Deleersnijder, Timescale methods for simplifying, understanding and modeling biophysical and water quality processes in coastal aquatic ecosystems: A review, Water 12 (10) (2020) 2717.

[2] E. Delhez, Transient residence and exposure times, Ocean Science 2 (1) (2006) 1–9.

[3] A. de Brauwere, B. De Brye, S. Blaise, E. Deleersnijder, Residence time, exposure time and connectivity in the scheldt estuary, Journal of Marine Systems 84 (3-4) (2011) 85–95.

[4] Z. Zainol, M. F. Akhir, Z. Zainol, Pollutant transport and residence time of a shallow and narrow coastal lagoon estimated using a numerical model, Marine Pollution Bulletin 164 (2021) 112011.

[2] https://toubkal.um6p.ma

[5] B. de Brye, A. de Brauwere, O. Gourgue, E. J. Delhez, E. Deleersnijder, Water renewal timescales in the scheldt estuary, Journal of Marine Systems 94 (2012) 74–86.

[6] F. Benkhaldoun, I. Elmahi, M. Seaïd, Application of mesh-adaptation for pollutant transport by water flow, Mathematics and Computers in Simulation 79 (12) (2009) 3415–3423.

[7] F. Benkhaldoun, I. Elmahi, M. Seaïd, Well-balanced finite volume schemes for pollutant transport by shallow water equations on unstructured meshes, Journal of computational physics 226 (1) (2007) 180–203.

[8] P. García-Navarro, J. Murillo, J. Fernández-Pato, I. Echeverribar, M. Morales-Hernández, The shallow water equations and their application to realistic cases, Environmental Fluid Mechanics 19 (2019) 1235–1252.

[9] L. Thiry, L. Li, E. Mémin, G. Roullet, Quasi-geostrophic projection of rotating shallow-water equations, arXiv preprint arXiv:2403.10199 (2024).

[10] N. T. Fourniotis, G. A. Leftheriotis, G. M. Horsch, Towards enhancing tidally-induced water renewal in coastal lagoons, Environmental Fluid Mechanics 21 (2021) 343–360.

[11] M. Jiang, Modeling water residence time and connectivity in the northern indian river lagoon, Estuaries and Coasts 46 (5) (2023) 1170–1189.

[12] F. Benkhaldoun, I. Elmahi, M. Seaïd, A new finite volume method for flux-gradient and source-term balancing in shallow water equations, Computer Methods in Applied Mechanics and Engineering 199 (49-52) (2010) 3324–3335.

[13] W. Aboussi, M. Ziggaf, I. Kissami, M. Boubekeur, A highly efficient finite volume method with a diffusion control parameter for hyperbolic problems, Mathematics and Computers in Simulation 213 (2023) 177–193.

[14] M. Ziggaf, I. Kissami, M. Boubekeur, F. Benkhaldoun, A well-balanced fvc scheme for 2d shallow water flows on unstructured triangular meshes,

Advances in Applied Mathematics and Mechanics 15 (5) (2023) 1335–1378. doi:https://doi.org/10.4208/aamm.OA-2022-0113.

[15] M. Maanan, M. Saddik, M. Maanan, M. Chaibi, O. Assobhei, B. Zourarah, Environmental and ecological risk assessment of heavy metals in sediments of nador lagoon, morocco, Ecological Indicators 48 (2015) 616–626.

[16] G. Umgiesser, C. Ferrarin, A. Cucco, F. De Pascalis, D. Bellafiore, M. Ghezzo, M. Bajo, Comparative hydrodynamics of 10 mediterranean lagoons by means of numerical modeling, Journal of Geophysical Research: Oceans 119 (4) (2014) 2212–2226.

[17] F. Ruiz, M. Abad, M. Olías, E. Galán, I. González, E. Aguilá, N. Hamoumi, I. Pulido, M. Cantano, The present environmental scenario of the nador lagoon (morocco), Environmental Research 102 (2) (2006) 215–229.

[18] J. R. Garratt, Review of drag coefficients over oceans and continents, Monthly Weather Review 105 (7) (1977) 915–929.

[19] K. M. Bryant, M. Akbar, An exploration of wind stress calculation techniques in hurricane storm surge modeling, Journal of Marine Science and Engineering 4 (3) (2016) 58.

[20] J. G. Zhou, Lattice boltzmann methods for shallow water flows, in: Springer-Verlag, Berlin, Springer, 2004.

[21] J.-F. Gerbeau, B. Perthame, Derivation of viscous Saint-Venant system for laminar shallow water; numerical validation, Ph.D. thesis, INRIA (2000).

[22] F. Marche, Derivation of a new two-dimensional viscous shallow water model with varying topography, bottom friction and capillary effects, European Journal of Mechanics-B/Fluids 26 (1) (2007) 49–63.

[23] D. Chu, J. Zhang, Y. Wu, X. Jiao, S. Qian, Sensitivities of modelling storm surge to bottom friction, wind drag coefficient, and meteorological product in the east china sea, Estuarine, Coastal and Shelf Science 231 (2019) 106460.

[24] C. Paugam, D. Sous, V. Rey, S. Meulé, V. Faure, O. Boutron, E. Luna-Laurent, E. Migne, Wind tides and surface friction coefficient in semi-enclosed shallow lagoons, Estuarine, Coastal and Shelf Science 257 (2021) 107406.

[25] O. Gourgue, E. Deleersnijder, L. White, Toward a generic method for studying water renewal, with application to the epilimnion of Lake Tanganyika, Estuarine, Coastal and Shelf Science 74 (4) (2007) 628–640.

[26] N. E. Monsen, J. E. Cloern, L. V. Lucas, S. G. Monismith, A comment on the use of flushing time, residence time, and age as transport time scales, Limnology and oceanography 47 (5) (2002) 1545–1553.

[27] S. Sahmim, F. Benkhaldoun, F. Alcrudo, A sign matrix based scheme for non-homogeneous pde's with an analysis of the convergence stagnation phenomenon, Journal of Computational Physics 226 (2) (2007) 1753–1783.

[28] R. Flather, A tidal model of the northwest european continental shelf, Mem. Soc. Roy. Sci. Liege 10 (1976) 141–164.

[29] G. D. Egbert, S. Y. Erofeeva, Efficient inverse modeling of barotropic ocean tides, Journal of Atmospheric and Oceanic technology 19 (2) (2002) 183–204.

[30] I. Kissami, Manapy: An mpi-based python framework for solving poisson's equation using finite volume on unstructured-grid, in: AIP Conference Proceedings, Vol. 3034, AIP Publishing, 2024.

[31] E. Deleersnijder, E. Delhez, Timescale-and tracer-based methods for understanding the results of complex marine models, Estuarine Coastal and Shelf Science 74 (2007).

[32] F. Maicu, B. Abdellaoui, M. Bajo, A. Chair, K. Hilmi, G. Umgiesser, Modelling the water dynamics of a tidal lagoon: The impact of human intervention in the nador lagoon (morocco), Continental Shelf Research 228 (2021) 104535.